A Microscale Solar Sail

Justin A. Atchison[i], Mason A. Peck[ii]
Sibley School of Mechanical and Aerospace Engineering
Cornell University, Ithaca, NY, 14853

We consider spacecraft length scaling as a means of enabling achieving passive, feasible infinite-impulse orbits. Taking inspiration from the orbital dynamics of dust, this paper discusses the consequences of length scaling on acceleration due to solar radiation pressure and demonstrates its effectiveness on a candidate microscale spacecraft. We propose to fabricate this dime-sized spacecraft on a single ultra-thin substrate of silicon. This choice reduces the total mass to fewer than 7.5 mg and makes the spacecraft bus itself a solar sail, yielding a lightness number β of 0.0175. This architecture can provide passive solar sail formations and various passive methods of changing orbital energy. The paper surveys and compares passive methods of achieving a marginally stable sun-pointing attitude including the addition of fixed vanes and optical grating of the surface. The microscale infinite impulse (MII) spacecraft design replaces the traditional spacecraft subsystems with a single integrated circuit (IC). Our current fabrication efforts are directed at realizing this spacecraft as a simple sensing and transmitting circuit with standard IC methods.

I. Introduction

DUST in the solar system experiences a surprising lifecycle. Solar pressure and electrostatic forces can compete with gravity to give very small particles highly nontraditional orbits. Some dust finds a stable orbit; some dust gently lands on the surface of planets like our own, and some dust is energetically ejected from the solar system.

Dust particles vary in size from a few molecules to 100 μm and have a mass smaller than a few μg. At these mass scales, the acceleration due to what would be considered perturbation forces on larger bodies can no longer be neglected. In fact, we propose that they be harnessed and manipulated in order to enable new propulsion techniques and missions. Dust's unique behavior motivates the present study of the orbital dynamics of extremely small bodies and the development of a spacecraft capable of exploiting on these physical principles.

In pursuit of this goal, we are working to create a self-contained "Microscale Infinite-Impulse" (MII) spacecraft capable of demonstrating significant, useful propellantless propulsion by virtue of its small length scale. Inspired by the simple, successful mission of Sputnik in 1957, we focus on a simple, feasible, but genuinely new design. For three weeks, the 23 inch diameter Sputnik I broadcast its internal temperature and pressure as it orbited and demonstrated the feasibility of artificial satellites. A half century later, we expect to duplicate Sputnik's achievement using less than one ten-millionth of its mass. Our design rethinks the traditional subsystems (power, propulsion, communications, etc) in an effort to produce a single silicon microchip spacecraft capable of infinite impulse.

Several other groups are actively and successfully developing monolithic integrated-circuit silicon spacecraft (sometimes called a "spacecraft-on-a-chip"), notably the Aerospace Corporation[1], Jet Propulsion Laboratories[2], and Surrey Space Centre[3]. The primary incentives for these research efforts are persuasive: economies of production, reduced launch mass, and distributed sensing opportunities. However, these objectives generally differ from our primary goal: capitalizing on length scaling to achieve feasible orbit control. These programs envision spacecraft with masses on the order of grams, which are no doubt unusually small by any traditional standard but are still a thousand times larger than our target. C. McCinnes[4] recognizes the promise of propellantless spacecraft designs which approach these length scales. He envisions smart, compact sails which use microelectromechanical systems (MEMS) to autonomously navigate the solar system. He further recognizes the challenges associated with long distance telecommunications for such small spacecraft. We pursue that shared vision first by surveying a variety of

[i] Graduate Research Assistant, jaa73@cornell.edu
[ii] Assistant Professor, mp336@cornell.edu

passive, feasible solar sailing opportunities for a candidate spacecraft. We then describe our design and fabrication progress to date.

II. Solar Radiation Pressure

Dust detectors on Pioneers 8 and 9 reported more dust impacts when facing the sun than when facing away. After measurement errors were ruled out, the spacecraft were found to be detecting streams of dust on outbound hyperbolic orbits. These streams of dust originate from comets, which shed dust throughout their orbit. When released near the sun, some dust experiences a sudden change in acceleration due to solar radiation pressure (SRP). If sufficiently large, this acceleration can unbound the orbit of these so-called β-meteoroids[5,6]. Here, acceleration due to SRP is assessed as a means of propelling a candidate MII spacecraft bus: a 25 μm thick, 1 cm square, 7.5 mg silicon microchip with integral solar cells and signal-transmitting circuitry. Section III describes this architecture in detail.

A. SRP Acceleration Scaling

As early as the 1920s Konstantin Tsiolkovsky and Fridrickh Tsander first realized that SRP can be manipulated to produce useful acceleration and can thereby achieve a class of spacecraft missions[4]. Rather than consider the "tremendous mirrors of very thin sheets" they envisioned, we consider solar pressure acting on this extremely small spacecraft. The pressure P from the sun due to momentum transfer from photons is

$$P = \frac{W}{c}\hat{\boldsymbol{r}}, \tag{1}$$

where c is the speed of light, W is the energy flux from the sun (units of J/m^{2}s), and $\hat{\boldsymbol{r}}$ is the direction of the position vector $\boldsymbol{r}$ with magnitude r. For a reflective flat plate exposed to the sun, the force $\boldsymbol{F}$ due to this solar pressure can be modeled by[4]

$$\boldsymbol{F} = 2\eta PA\left(\cos^2\alpha\right)\hat{\boldsymbol{n}}, \tag{2}$$

where A is the area of the plate exposed to photons when facing sunward, and α is the sail pitch angle defined by the plate's normal unit vector $\hat{\boldsymbol{n}}$ and the direction of the incoming photons $\hat{\boldsymbol{e}}_i$ as shown in Figure 1. The η<1 term accounts for a surface's non-ideal optical properties associated with absorption and diffuse reflection. The $\cos^2\alpha$ term accounts for area projection in the radial (sunward) direction and the off-radial photon reflection $\hat{\boldsymbol{e}}_r$. This simplified force model provides insight into the behavior at small scales. It is particularly appropriate in the case of the MII spacecraft because flatness is easily achieved, in contrast to much larger sails that billow and wrinkle.

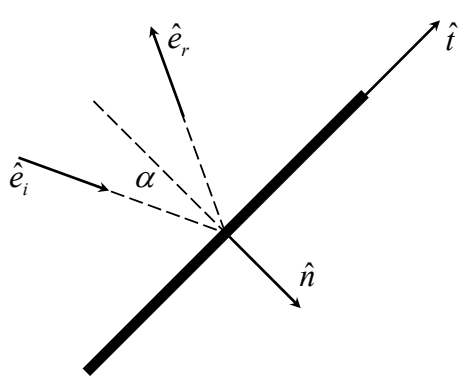

Figure 1. Vector directions for solar sails.

The incident flux is modeled with an inverse-square law

$$W = W_0 \left(\frac{r_0}{r} \right)^2 , \tag{3}$$

where W_0 is a reference magnitude at a reference distance r_0. The force due to solar pressure is purely radial on a sail with constant pitch angle and decreases with an inverse-square dependence, just as the force due to gravity F_G. This similarity motivates the dimensionless parameter β, known as the lightness number, which measures a sail's effectiveness. β relates the magnitude of SRP acceleration to the magnitude of gravitational acceleration

$$\beta = \frac{F_{SP}}{F_G} = \frac{2W_0 r_0^{\ 2} \eta}{\mu c \sigma} , \tag{4}$$

where μ is the sun's gravitational constant and σ is the *loading parameter*

$$\sigma = \frac{m}{A} . \tag{5}$$

The loading parameter relates the mass of the body m to its sail area and is a function of the geometry and material of the body. Our MII spacecraft resembles a flat plate. For such a shape, with its maximum area normal to the sun, the loading parameter is

$$\sigma = \frac{m}{A} = \frac{\rho l^2 d}{l^2} = \rho d , \tag{8}$$

where l is the plate's side length and d is the plate's thickness. Reducing the thickness of the plate (rather than side length) increases β. These simple results motivate the concept of a plate shaped integrated circuit spacecraft whose small depth enables it to function as a solar sail.

B. Passive SRP Orbit Designs

In an effort to both maximize and benefit from SRP acceleration, we evaluate passive and scalable orbit designs. Here, *passive* indicates that these solutions do not require any form of active feedback control. We evaluate two classes of available orbits, those that maintain a constant β and those that use a time-varying β to alter orbital energy.

1. Constant β Orbits

This first application describes the simplest SRP enabled passive formation: spacecraft with constant β in a heliocentric, circular orbit. An expression for energy leads to the result that the angular velocity ω of a body in a heliocentric circular orbit is modified by the lightness number[4]

$$\omega = \sqrt{\frac{\mu(1-\beta)}{r^3}} . \tag{9}$$

Alternatively, this result can be expressed in terms of orbital radius (in this case for $\beta < 1$)

$$r = \left(\frac{\mu(1-\beta)}{\omega^2} \right)^{\frac{1}{3}} . \tag{10}$$

That is, the circular radius for a certain angular velocity is reduced in response to a reduction in gravity's radial force.

These two principles of circular orbits lead to novel satellite formations. Solar pressure allows two satellites to orbit with the same angular velocity at unique radii. Alternatively, two spacecraft can orbit at the same radius, but with unique angular velocities, perhaps to spread out azimuthally along an orbit[4]. These two applications are illustrated in Figure 2 below, where Body A is a point mass and Body B has a nonzero lightness number. Figure 3

gives sample values for along-track motion $\Delta\theta$ (illustrated in Figure 2b) for a heliocentric circular orbit at 1 AU. This orbit requires a constant lightness number that we propose to achieve with a passively stable sun-pointing architecture.

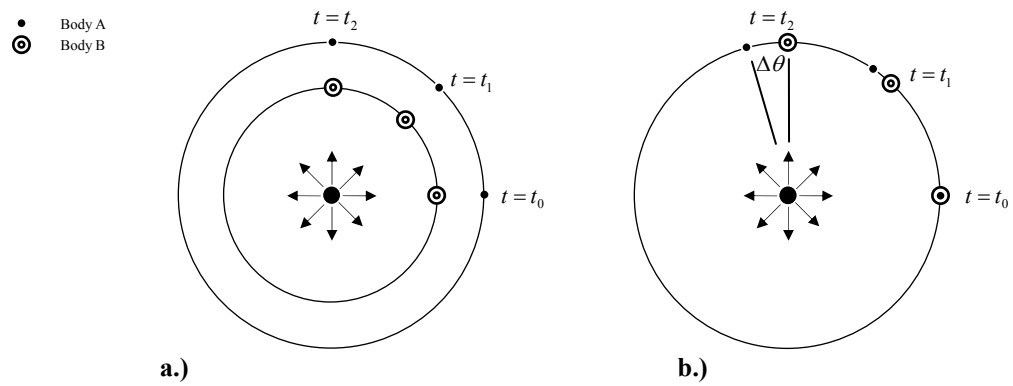

Figure 2. Deviations from non-Keplerian orbits by solar sails in circular equatorial orbits. a.) constant-radius formation flying and b.) along-track separation

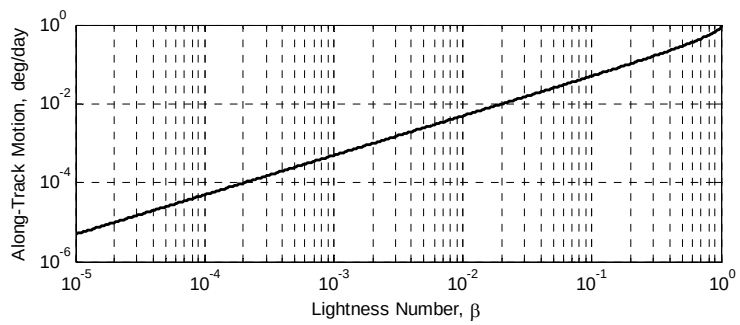

Figure 3. Along-track motion in deg/day between a point mass spacecraft and a constant lightness number (β) spacecraft in heliocentric circular orbit at 1 AU.

2. Time-Varying β Orbits

A constant lightness number results in constant orbital energy. Figure 4 shows the directions of the solar pressure force $\hat{\boldsymbol{n}}$ and velocity $\hat{\boldsymbol{v}}$ for a flat, inertially fixed-heading plate throughout the course of an elliptical orbit. Like in a Keplerian orbit, energy added in one half of the orbit (where $\hat{\boldsymbol{n}} \cdot \hat{\boldsymbol{v}} > 0$) is removed in the second half (where $\hat{\boldsymbol{n}} \cdot \hat{\boldsymbol{v}} < 0$).

If, however, the lightness number varies (e.g. by actuation) over the course of an orbit, the net energy can be manipulated. The β-meteoroids for example, naturally achieve escape velocity via a variable lightness. This dust originates from a larger body, such as a comet, whose lightness number is negligible. As the dust separates from the body, its new loading parameter (a function of the individual particle's size rather than the comet's size) takes effect and it experiences sufficient acceleration to unbound its orbit[7].

The lightness number of a plate-shaped MII spacecraft can be actuated by modulating the reflectivity of its two sides. For example, a spacecraft with a highly reflective material coating one side and a highly absorptive material coating the other sees a variation in energy throughout its orbit. Figure 5 shows the normalized radial and tangential accelerations for the candidate MII spacecraft throughout a circular orbit. The constant-β line represents the normalized acceleration magnitude for an MII spacecraft with two identically reflective sides (η = 0.85, β = 0.0175). The variable-β line represents the acceleration on a plate with two different coatings. One side is reflective, and the second side is perfectly absorptive (η = 0.50, β = 0.0103), such that it acts like a black body. Further, Figure 6

shows the resulting semi-major axis (i.e. energy) and eccentricity over the course of the orbit, demonstrating that the net energy and eccentricity change over the orbit for the dual-coated case. By reversing the orientation of the plate or the grade of the orbit, energy and momentum can be removed rather than added.

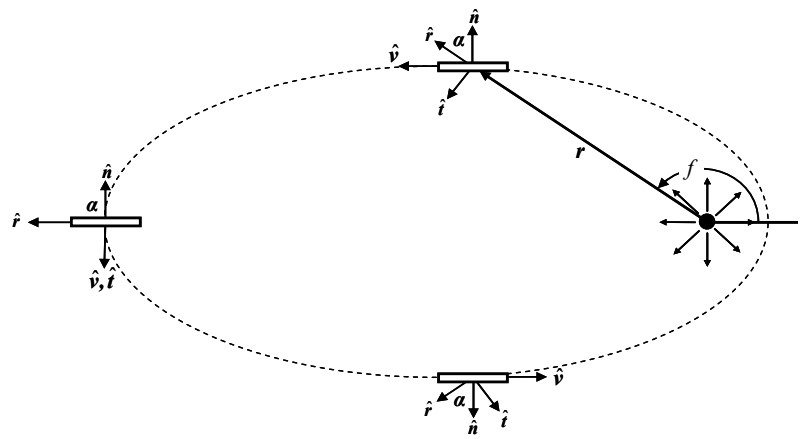

Figure 4. Arbitrary posigrade elliptical orbit with velocity vectors and solar pressure vectors (acting in $\hat{n}$).

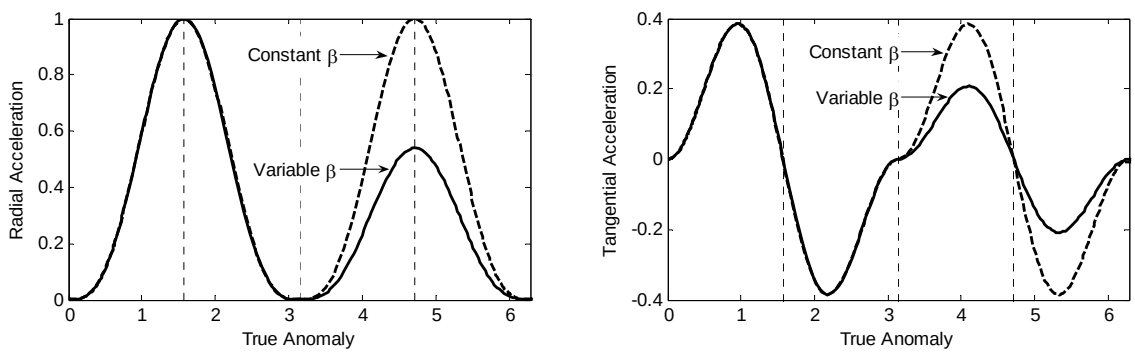

a.) **b.)**

Figure 5. a) Normalized radial and b) tangential acceleration over a single circular orbit at 1 AU for two fixed-attitude MII spacecraft: one with two reflective (η = 0.85) sides (dashed line) and another with a reflective side (η_1 = 0.85) and a perfectly absorbing side (η_2 = 0.5).

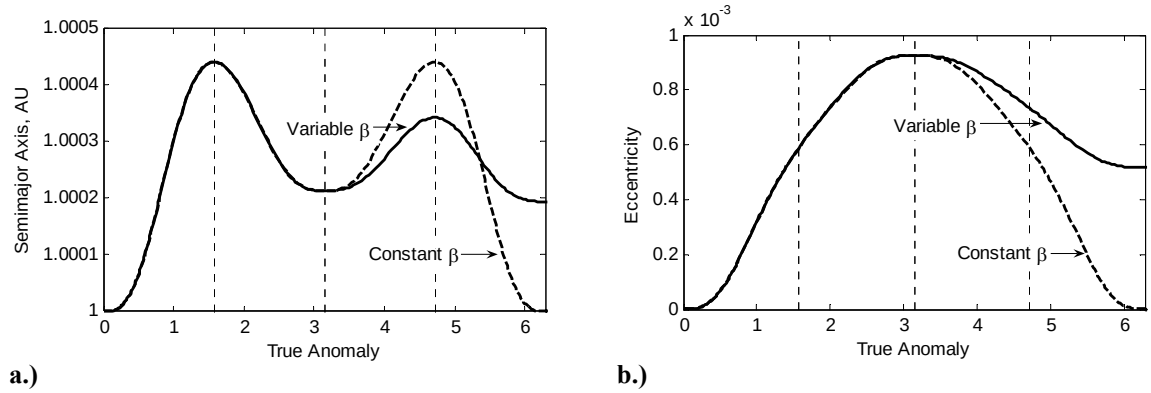

a.) **b.)**

Figure 6. a.) Semi-major axis and b) eccentricity over a single circular orbit at 1 AU for two fixed-attitude MII spacecraft: one with two reflective (η = 0.85) sides (dashed line) and another with a reflective side (η_1 = 0.85) and a perfectly absorbing side (η_2 = 0.5). The rightmost points show the cumulative change over a one year period.

The surface of an MII spacecraft is populated with integrated circuit (IC) components including solar cells; so, we cannot arbitrarily apply reflective or absorptive coatings. Equation 8 indicates that increasing the side length of a flat plate does not affect the loading parameter. This result implies that the 1 cm^2 MII design can be fabricated onto a square larger than 1 cm^2 without loss of β. The coatings can be applied to this additional surface area

C. Passive Attitude Control

Using thin film fabrication techniques, the MII vehicle is designed such that the spacecraft itself is a sail. The direction of the SRP acceleration is coupled to its attitude via the pitch angle. With neither active attitude control nor spin stabilization, the body's attitude is easily disturbed by torques associated with environmental phenomena such as free molecular flow, magnetic fields, gravity gradient effects, dust/meteoroid impingement, and SRP. Precisely centering the spacecraft's center of mass and center of pressure likely poses a challenge in for this scale of spacecraft. As discussed below, this offset results in disturbance torques. We survey three options that use SRP to mitigate these disturbances and maintain a known attitude, which fixes β. We also briefly evaluate spin stabilization for orbits that exploit an inertially fixed heading to produce a variable β.

1. Separation of the Centers of Mass and Pressure

An SRP disturbance torque is produced when the center of pressure $\boldsymbol{r}_{cp}$, where the effective SRP force acts, is displaced from the center of mass $\boldsymbol{r}_{cm}$ [8]. An equilibrium attitude (or angle) with respect to the sun line is defined by the relative positions of these two locations. The sail is said to be statically balanced when $\boldsymbol{r}_{cp}$ is located between the sun and $\boldsymbol{r}_{cm}$ [9,10]. The center of mass $\boldsymbol{r}_{cm}$ in body fixed coordinates along an arbitrary direction $\hat{\boldsymbol{x}}$ is found from the integral of the density distribution $\rho(x)$ over the length l of the plate

$$\boldsymbol{r}_{cm} \cdot \hat{\boldsymbol{x}} = \frac{\int_l x\, \rho(\boldsymbol{x})\, dx}{m}. \tag{11}$$

Likewise, the center of pressure $\boldsymbol{r}_{cp}$ is found from the integral of the SRP force distribution $\boldsymbol{F}(x)$

$$\boldsymbol{F}(x) = 2P\, \eta(x)\, d(x) \left(\cos^2 \alpha(x)\right) \hat{\boldsymbol{n}}(x), \tag{12}$$

$$\boldsymbol{r_{cp}} \cdot \hat{\boldsymbol{x}} = \frac{\int_l x\,\boldsymbol{F}(x)dx}{\int_l \boldsymbol{F}(x)dx}. \tag{13}$$

Here, the reflective efficiency, depth d, pitch angle, and normal direction are functions of the coordinate x along the direction $\hat{\boldsymbol{x}}$. In some of the architectures below, these terms are varied as a means of changing the value of $\boldsymbol{r_{cp}}$. For systems described more conveniently as a set of n_f discrete plates with constant parameters, the following discrete expressions may be used:

$$\boldsymbol{r_{cm}} \cdot \hat{\boldsymbol{x}} = \frac{\sum_{i=1}^{n_f} m_i x_{cmi}}{\sum_{i=1}^{n_f} m_i}. \tag{14}$$

$$\boldsymbol{r_{cp}} \cdot \hat{\boldsymbol{x}} = \frac{\sum_{i=1}^{n_f} \eta_i d_i \left(\cos^2 \alpha_i\right) w_i x_{cpi} \hat{\boldsymbol{n}}_{\boldsymbol{i}}}{\sum_{i=1}^{n_f} \eta_i d_i \left(\cos^2 \alpha_i\right) w_i \hat{\boldsymbol{n}}_{\boldsymbol{i}}}. \tag{15}$$

Here, w_i, d_i, $x_{cmi,}$ and x_{cpi} are the ith plate's width, depth, and centers of mass and pressure in the $\hat{\boldsymbol{x}}$ direction, respectively. The resulting SRP torque is

$$\boldsymbol{\tau} = \left(\boldsymbol{r_{cp}} - \boldsymbol{r_{cm}}\right) \times \boldsymbol{F}. \tag{16}$$

For noncollocated centers constrained to the plane of a thin plate, this torque is zero only when $\boldsymbol{F}$ is zero, i.e. when the pitch angle is 90°. The sun-pointing heading is therefore unstable for a thin plate, in that an arbitrarily small distance of the mass center from the center of pressure causes the attitude angle to diverge from 0°. While 90° is itself a passively stable solution, it doesn't offer access to solar pressure or solar power. So, it is not desirable. To achieve equilibrium angles other than 0° and 90°, the centers must be displaced in both the tangential and normal directions of the plate. Such displacement is challenging for the extremely thin architecture we are proposing.

The attitude motion is undamped and therefore oscillates indefinitely about an equilibrium angle and rotates about its sun line. So, a constant nonzero equilibrium angle does not correspond to a constant nonzero pitch angle. A force cannot produce a torque along its direction. So, there is no simple architecture that can offer a direct SRP generated restoring torque. For the same reason, gravity gradient cannot be used to constrain this remaining degree of freedom. The Team Encounter solar sail design uses a fixed offset of centers to establish a desired sun line, and an active control system to achieve a constant pitch angle. The system uses a star camera as an input and gimbaled reflective vanes as an output[8,11,12]. This architecture is a simple means of achieving a logarithmic spiral trajectory, and encourages research into passive means of constraining the final rotational degree of freedom.

2. Corner-Cube Sun-Pointing Attitude

An extension of the architecture described above establishes a sun-pointing equilibrium angle and constant lightness number by connecting three of the plate-like MII spacecraft together to form the corners of a cube, as shown in Figure 11. This approach is analogous to changing the parameters $\alpha(x)$ and $\hat{\boldsymbol{n}}(x)$ in Esq. 12. Kirpichnikov et al.[13] and van de Kolk and Flandro[14] have rigorously demonstrated that this geometry creates a marginally stable sun-pointing attitude whose nonradial force components cancel in 2D and 3D orientations. SRP torque orients the body such that the three plates' common corner reaches an equilibrium angle with respect to the sun line. For uniform, equal-length plates contemplated here, the axis from the center of mass to the common corner points directly at the sun.

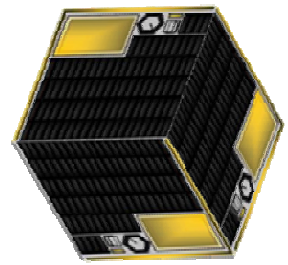

Figure 7. Stable, sun-pointing corner-cube architecture.

One may be tempted to reorient the spacecraft such that it forms a concave corner-cube retroreflector. This geometry reflects light directly back towards the sun, maximizing the solar pressure's effect for the given area, and cancelling one of the cos(α) terms in Equation 2. However, this equilibrium orientation is unstable without active control[13].

The disadvantage of the stable architecture is a less effective loading parameter:

$$\sigma = \frac{m}{A} = \frac{3\rho l^2 d}{\frac{3}{\sqrt{3}} l^2} = \sqrt{3}\rho d \cdot \tag{17}$$

An architecture that uses three of the candidate MII spacecraft yields a loading parameter of 0.1295 kg/m^2 and a lightness number of 0.010. This architecture has the added benefits of redundancy and increased antenna transmission coverage. Some differentiation among the chips may also improve functionality.

3. Grated-Plate Sun-Pointing Attitude

We also consider grating the plate's surface in order to produce a stable sun-pointing equilibrium. With grating, the surface of the plate can be constructed such that the location of the center of pressure is a function of the pitch angle. J. Falcovitz[15] explored this option in the context of using solar arrays for attitude control. Here we develop a model from first principles and evaluate its effectiveness.

The model illustrated in Figure 13 gives n_f plate "fins" of different optical efficiencies (η_0,η_1, and η_2) and depths d_i (measured into the page in Figure 13) symmetrically distributed along the plate's surface and aligned in the plate-normal direction. The goal is to design a surface profile that gives an asymmetric projection in the direction of the sun line as the pitch angle changes. In this case, the center of pressure changes due to shadowing and secondary reflection. This analysis follows from Eq. 14-16. After algebraic simplification, the torque is

$$\boldsymbol{\tau} = \begin{pmatrix} 2P\eta_0 b_f \left((\eta_1 - \eta_2)\sum_{i=1}^{n_f}(d_i x_{cpi}) + (2+\eta_1+\eta_2)\left(w_f + \frac{b_f}{2}\right)\sum_{i=1}^{n_f}(d_i)\mathrm{sgn}(\alpha) \right)\cos^2\alpha - \\ 2P\left(\frac{h_f^{\,2}}{2}(1+\eta_0)(\eta_1+\eta_2)\right)\sum_{i=1}^{n_f}(d_i)\mathrm{sgn}(\alpha)\sin^2\alpha \end{pmatrix}(\hat{\boldsymbol{n}}\times\hat{\boldsymbol{t}}) \tag{19}$$

where $b_f = h_f \tan(\alpha)$ is the projected length of each fin's shadow.

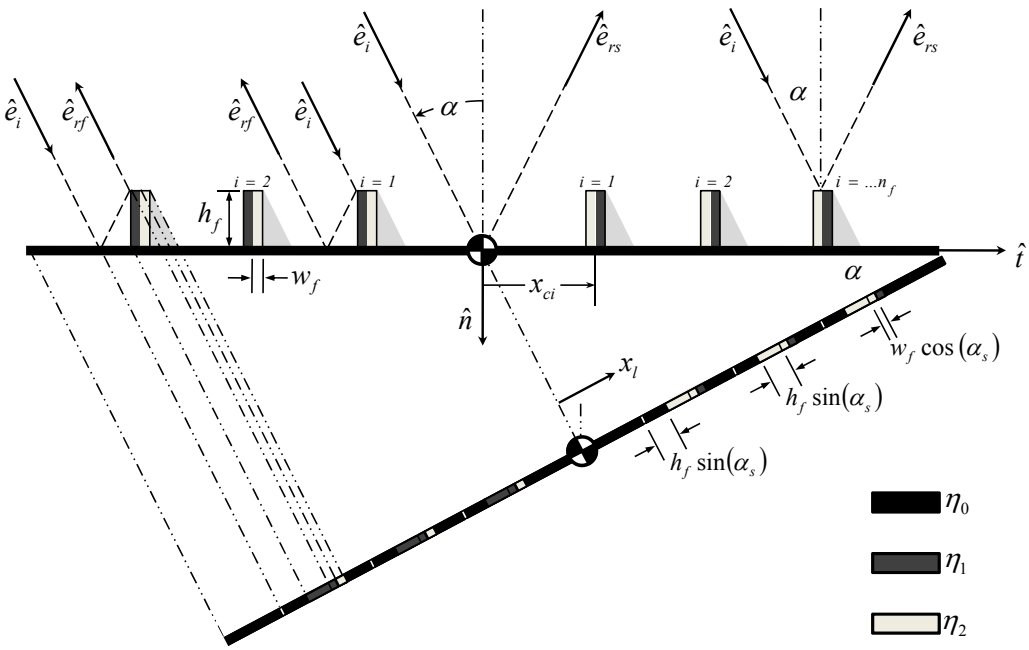

Figure 8. Plate model with optical grating illustrated as discrete plates aligned with the plate-normal direction.

The signum function ensures that force acting on the fins is directed properly with respect to the direction of α illustrated in Figure 13. The model is valid over a limited range of pitch angles $\pm\ \alpha_r$, which is defined by the fin dimensions and the spacing between the fin centers Δx_{ci}

$$\alpha_r = \arctan\left(\frac{\Delta x_{ci} + 2w_f}{h_f}\right). \tag{20}$$

The model does not properly account for reflection and shadowing at pitch angles outside of this range.

The large number of parameters in Eq. 19 limits its value for providing insight. It can be simplified by letting $d_i = l$ and assuming the aspect ratio of the fins is high, $h_f >> w_f$. The result is somewhat more tractable.

$$\boldsymbol{\tau} = \begin{pmatrix} 2P\eta_0 b_f l\left((\eta_1-\eta_2)\sum_{i=1}^{n_f}(x_{cpi}) + (2+\eta_1+\eta_2)\frac{b_f}{2}n_f\,\mathrm{sgn}(\alpha)\right)\cos^2\alpha - \\ 2P\left(\frac{h_f^{\,2}}{2}(1+\eta_0)(\eta_1+\eta_2)n_f l\right)\mathrm{sgn}(\alpha)\sin^2\alpha \end{pmatrix}(\hat{\boldsymbol{n}}\times\hat{\boldsymbol{t}}) \tag{21}$$

One can conclude that torque is driven to zero at zero pitch. Evaluating the model with $\eta_0 = \eta_1 = \eta_2 = \eta$

$$\begin{aligned}\boldsymbol{\tau} &= \left(b_f^{\,2}\eta l\, n_f(1+\eta)\cos^2\alpha - h_f^{\,2}\eta l\, n_f(1+\eta)\sin^2\alpha\right)(\hat{\boldsymbol{n}}\times\hat{\boldsymbol{t}}) \\ &= 0\end{aligned} \tag{22}$$

indicates that the relative difference in coatings is essential in order to generate a torque.

Figure 14 shows the torque from Equation 21 evaluated for a 1 cm square plate with a total of 50 fins spaced 100 μm apart, starting from the outer edge. Each fin is 100 μm tall and assumed to be of negligible width. Each fin surface is modeled with an efficiency of either 0.85 or 0.75 as the labels indicate. The figure confirms the conclusion following Equation 22. The difference in efficiencies on each side of the fins dominates the direction

and magnitude of the torque. Stable solutions about the sun-pointing axis are shown. These sets of optical efficiencies produce restorative torques for deviations in pitch. This architecture is potentially useful because it suggests passive sun-pointing stability with the addition of relatively little mass.

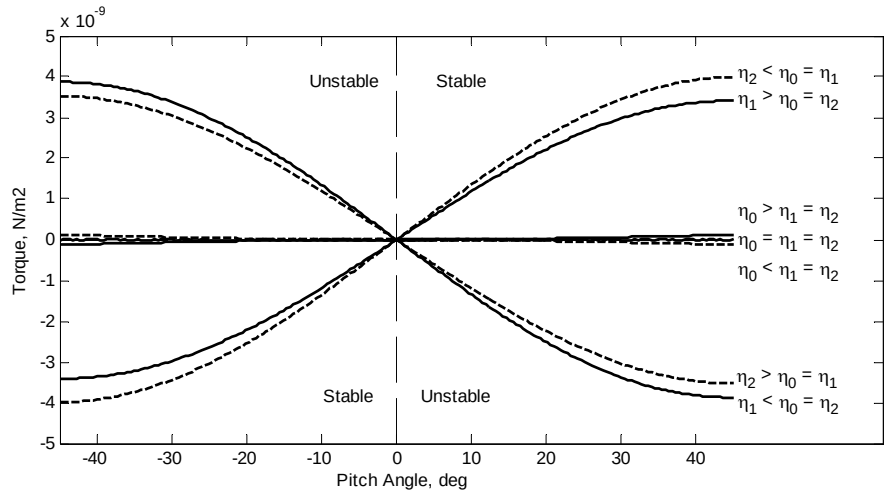

Figure 9. Relative magnitude and direction of torque for reduced grated plate model with l = 1cm, h_f = 100 µm, n_f = 25, and η_i = 0.85 or 0.75.

4. Inertially Fixed Heading

The above architectures are based on spacecraft whose attitude is fixed relative to the sun and yield a constant lightness number. For energy change maneuvers, a variable lightness number and inertially fixed reference is needed. An inertially fixed heading can be achieved by spinning the spacecraft about its maximum axis. This spin gives the plate dynamic stability. Misalignment of the center of mass from the center of pressure produces a body-fixed torque that precesses the spacecraft's angular momentum vector about the sun line. The maximum acceptable precession angle establishes the minimum required spin rate. A spin rate of 8 rpm restricts the precession to 10° for a 1 mm tangential misalignment using characteristic inertia values for our MII design in the small-angle regime[8].

III. Candidate Microscale Infinite-Impulse Spacecraft Bus

Having motivated length scaling of spacecraft, we now explore how small a functional spacecraft can be feasibly produced. Others have asked this same question at a high level and have developed "systems-on-chip," which integrate traditionally separate components into a single integrated circuit (IC) package. The result is a low-cost, light-weight, easily-reproducible chip that accomplishes the same tasks as its conventional large-scale counterpart. The next logical step for this technology is to apply the same techniques to an entire spacecraft to create a "spacecraft-on-a-chip," as we and several others are currently pursuing, though with different motivations and strategies[3].

We approach this task from a feasibility standpoint, intending to demonstrate functionality at the scales of interest to our dynamic analyses. Thus, we approach the design space with an emphasis on simplicity, achievability, and scalability, rather than with an interest in advancing the state of the art in microfabrication. Our goal is to design an extremely small demonstration spacecraft bus, in which we can incorporate the propellantless-propulsion architectures described above. In keeping with spacecraft-design convention, we describe this candidate spacecraft bus in terms of traditional subsystems. The baseline design, shown in Figure 15, has five primary components. Each of these components is described below in detail in the discussion of its respective subsystem.

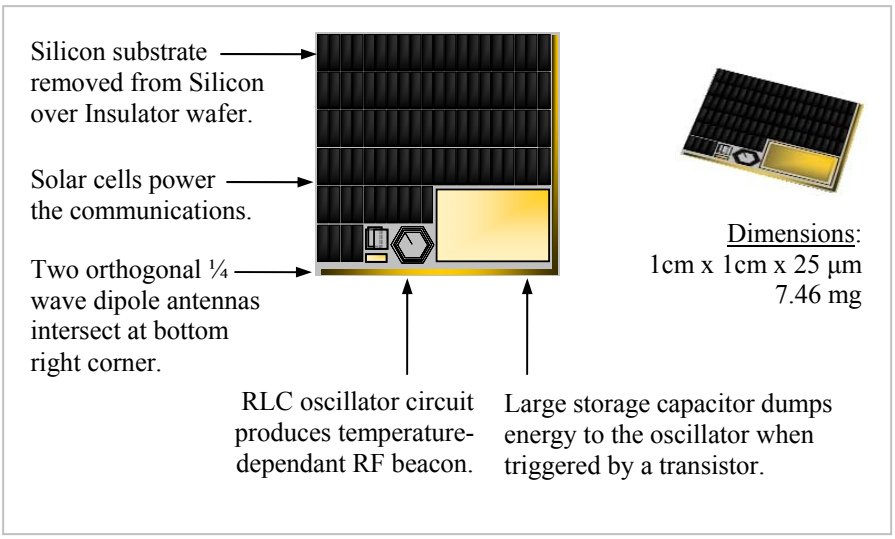

Figure 10. Current MII bus layout with dimensions.

A. Propulsion

Traditional propellant mechanisms such as chemical or ion thrust systems cannot be easily scaled to the IC level. A novel exception is so called "digital propulsion". Lewis, et al. have successfully fabricated and demonstrated a device that delivers discrete amounts of thrust using microscopic chambers and chemical propellant[16]. Though digital propulsion may prove relevant for our research in the long run, our current research is motivated primarily by propellantless propulsion, in hopes of enabling otherwise impossible missions and orbits. SRP, as described above, is among the potential propellantless-propulsion approaches.

B. Attitude Determination and Control

This paper has surveyed methods of achieving stable attitude orientations using passive SRP and spin stabilization. The sun-pointing architectures require a particular design and fabrication. Once released into an orbit, they behave passively. The momentum-stabilized architecture requires a method of spinning each chip about its major axis. A conceptually simple but perhaps costly solution is to design a mechanism to both spin and deploy each chip once in space. Alternatively, we are exploring outgassing as a means of producing torque. In this architecture, volatile material deposited on the edges of each chip would outgas in the vacuum of space to impart angular momentum, without the need for a spinning-deployment mechanism. Future research will also consider active control, perhaps with micro-electro-mechanical systems (MEMS) as proposed by McInnes[4].

C. Structure

The structure of the spacecraft consists of the volume of semiconductive substrate on which the other subsystems are fabricated. A gallium-arsenide substrate offers desirable radiation hardening and the opportunity to produce high efficiency solar cells. However, the cost of integrating MEMS subsystems on gallium arsenide may discourage its use. We therefore focus on a more common, silicon substrate. At 2300 kg/m^3, solid Silicon is significantly denser than 100 kg/m^3, the net density of a typical spacecraft[17.] Nevertheless, the silicon substrate offers the most near-term opportunity to decrease total mass.

Like traditional structural subsystems, the substrate must support and mechanically interface the other subsystems, facilitate ground handling, and withstand vibrations during transportation and launch. The MII design is less concerned with vibration control because the natural frequencies of such a structure are be far higher than the likely attitude-control bandwidth of any launch vehicle and the MII itself . Instead, the design is based on the lightest structure on which components can be fabricated: the thinnest possible substrate for a required surface area. For polished silicon wafers, this limit is approximately 200 µm. Thinner silicon is too brittle to machine. Silicon-on-Insulator (SOI) wafers are an alternative. Such wafers consist of an ultra-thin layer of silicon on top of a silicon-oxide layer. This substrate offers structural rigidity and handling during fabrication, after which the silicon-oxide

layer can be removed to leave the processed device on the ultra-thin silicon layer. Then, arbitrarily thin silicon can be produced, although the thickness in this paper is restricted to no less than 25 μm for conservatism.

We estimate that sufficient functionality can be achieved in 1 cm^2. In order to maximize use of the surface area, we consider flip-chip fabrication. In this process, two chips are manufactured such that their backsides can be mated and both chips face outward. This technique allows the MII spacecraft to incorporate devices whose fabrication techniques are incompatible by producing them separately and integrating them as a final step. Of primary interest is the placement of solar cells on both sides of the chip to ensure that power is always available, regardless of attitude.

The mass of such a 1 cm^2 silicon substrate is 5.75 mg. For conservatism, the mass budget includes 30% margin, yielding a total mass of 7.46 mg, which is used in this paper's calculations. The silicon fabrication process consists of additive and subtractive processes, which add or remove material from the substrate to form a device. The net contribution of these processes is assumed to be negligible.

D. Power

Solar cell power generation is both passive and based in semiconductor physics, making it a natural choice for power in this application. We focus on silicon-based, first-generation solar cells, which use a single-layer p-n junction diode to pass photovoltaic currents. With sets of individual cells strategically connected in parallel or series, an array can be designed with specific voltage and current characteristics to accommodate propulsive, attitude control, or payload requirements. Commercially available, high-efficiency cells commonly achieve specific power on the order of 200 W/kg. Integrated solar cells are much less efficient[3]. This inefficiency drives the design to devote the majority of the available silicon surface to photovoltaics. Likewise, electrochemical batteries are difficult to integrate. It may be that an MII spacecraft will simply be powerless in eclipse. Alternatively, thin film capacitors printed on the chip might be used to store power. Solar cells produce electric power proportional to the cosine of the pitch angle. For this reason, sun-pointing attitude solutions offer an important advantage over other attitudes.

E. Communications

Following Sputnik's example and facing the challenges of little available power, we conceive the communications subsystem as a transmit-only beacon. The data consists of a single beep at a single frequency—a binary output based on the presence or absence of the carrier. There is no signal *per se* carried on that frequency. For this simple transmission to be tracked from a ground station, it must be powerful enough to overcome free-space loss, atmospheric attenuation, and other noise sources. The communication link's carrier-to-noise-ratio *C/N* is therefore a useful measure of goodness. This ratio is influenced by the signal's frequency, the orbit's altitude, the transmitter's losses and power, atmospheric conditions, and antenna efficiency. A single chip can accomplish only so much. A simple way to close the link budget is to select a ground station with high enough gain. For example, a candidate ground segment might use one of the Deep Space Exploration Society's two 60 foot diameter parabolic dishes located in a radio-quiet region of Colorado. With an antenna gain of 32 dB, this dish represents an extremely sensitive publicly accessible receiver. Roughly speaking, a *C/N* of 10 at 8 GHz requires only 5 mW of emitted power to reach ground from LEO.

A simple RC-tank charging circuit can produce periodic bursts of power. In the baseline architecture, solar power charges a capacitor until a critical voltage is reached and a transistor is opened, releasing the stored energy. This energy is sent through an LC oscillator and is emitted as RF energy via two antennas. This sequence results in a pulsed oscillating signal. When sunward, the spacecraft exhibits an 8 s charging constant. The performance of RLC circuits depends on temperature, implying that the pulse frequency will vary with temperature. This dependence can be modeled or characterized experimentally and used to infer temperature from the beacon's center frequency.

Thin-film deposition allows the fabrication of multilayered parallel-plate capacitors directly alongside other IC components. Alternately deposited layers of metal and dielectric can store charge efficiently in a small surface area. Area-capacitance density serves as a metric in allocating the surface area of our wafer.

The antenna can be printed directly on the spacecraft bus or connected as a thin filament. Since the candidate MII bus does not include active attitude control, directionality cannot be a requirement. For antenna printing, two antenna styles seem most practical, having been fabricated and demonstrated at our size scales: a linear dipole antenna and a loop dipole antenna. Dipole antennas can be designed for a resonant frequency by sizing the length at full, half, or quarter wavelengths. In the case of a quarter-wave dipole, a centimeter-length limit constrains the minimum antenna resonant frequency to approximately 7.5 GHz. The second option, a loop antenna, offers increased gain over a dipole but also has equally restrictive frequency limits. For example, a 1 cm x 1 cm square

loop yields a minimum resonance of approximately 8 GHz. Based on frequency allocation, ground-station capabilities, and atmospheric attenuation, these minimum frequencies drive the transmitter's design.

Barnhart[3] notes that it is infeasible to track such a small spacecraft using radar. By contrast, our proposed architecture features a beacon that transmits continuously, and it therefore serves as an onboard, powered Radio-Frequency Identification (RFID) which operators can use to tune the receiver during the first few passes.

F. Thermal Control

In orbit, this spacecraft's low thermal mass will result in temperatures between -130°C and 100°C. This variation can occur within tens of seconds[17]. Thermal stresses associated with eclipses may fatigue the chip where dissimilar metals contact. These risks, along with possible remediative strategies such as microfabricated radiator fins, have yet to be evaluated. An active means of remediation might be achieved by spinning the bus: tilting the attitude so that the face points toward or away from the sun or the earth at an angle that optimizes combined power and thermal performance.

G. Payload

The final subsystem we consider is the spacecraft payload. In keeping with this simple, feasible, highly integrated design, the one-way communications beacon serves as a means of transmitting spacecraft position and temperature. The orbit can be estimated after multiple pulses have been recorded. Position time histories then allow operators to evaluate the effectiveness of the solar sail. The estimated frequency of the pulses communicates the temperature of the analog communications circuit. We emphasize that this early phase demo may be followed by other applications, with considerably more sophisticated payloads.

IV. Current Fabrication Process

We are developing a simple hardware demonstration of the MII bus in the Cornell NanoScale Science & Technology Facility (CNF). Our most recent efforts have focused on the RLC oscillator. Having achieved our target 10 nF/cm^2 capacitance density using silicon-dioxide as a dielectric layer, we are fabricating a series of inductors based on a three-layer octagonal design by Craninckx[18]. Figure 16 shows a photograph of our current oscillator at 20x magnification. Concurrently, members of our group are exploring the challenges associated with solar cell integration and have begun fabrication on organic solar cells which are compatible with many other fabrication processes. Once the chip is fabricated, we will begin thermal vacuum chamber and sun simulator testing.

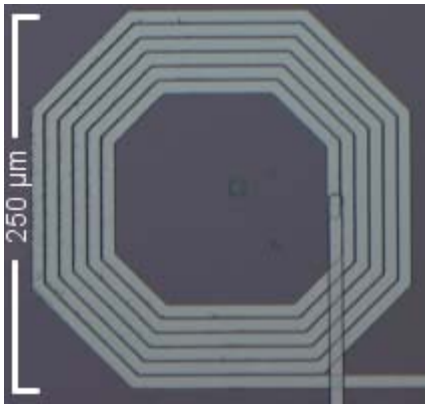

Figure 11. A 6 loop, 240 µm wide octagonal inductor for the RLC oscillator is shown at 20x magnification.

V. Conclusions

This paper presents motivation, analytical evaluation, supporting simulation, and sample designs for a microscale infinite-impulse (MII) spacecraft with sufficiently low mass to enable solar sailing. The candidate bus is a 1cm x 1cm x 25 µm silicon IC that conservatively weighs less than 7.56 mg. Each conventional spacecraft subsystem is accounted for and described in the context of a Sputnik inspired temperature sensing mission.

If paired with two other MII spacecraft to form a corner cube, this design can passively reduce the effect of gravity by 1.0% via solar pressure, enabling unique formation opportunities. Using an optical grating scheme to produce stable sun-pointing attitudes, this acceleration can be improved up to 1.75% of gravity. If spin-stabilized and strategically coated with absorptive (η = 0.5, β = 0.0103) and reflective (η = 0.85, β = 0.0175) materials, the spacecraft can passively gain or remove energy and momentum in a simple circular orbit.

Although the lightness numbers are similar to traditional solar sail designs, the passive energy-change maneuver using different coatings is much less efficient than a simple logarithmic spiral trajectory. Nevertheless, we emphasize that the difficult engineering challenges associated with a 22,700 m^2 spacecraft introduce risk and cost that the 1 cm^2 MII trades for small size.

Dramatically reducing a spacecraft's mass by replacing the system with a single integrated circuit enables us to capitalize on these perturbations and feasibly accomplish infinite-impulse missions. The next steps in the proposed work include completing the demonstration chip and evaluating its performance in a terrestrial testbed environment.

Acknowledgments

J. Atchison wishes to thank Alfred Ernst of Cornell University for extensive fabrication work.

This work was funded in part by the National Defense Science Engineering Graduate Fellowship and the NASA Institute for Advanced Concepts (Grant 07605-003-071).

This work was performed in part at the Cornell NanoScale Facility, a member of the National Nanotechnology Infrastructure Network, which is supported by the National Science Foundation (Grant ECS-0335765).

References

1.Janson, S.W., "Mass-producible silicon spacecraft for 21st century missions," *AIAA Space Technology Conference & Exposition, Albuquerque, NM,* 1999.

2.Miller, L.M., "MEMS for space applications," *Proceedings of SPIE,* Vol. 3680, 2003, pp. 2.

3.Barnhart, D., Vladimirova, T., and Sweeting, M., "Very-Small-Satellite Design for Distributed Space Missions," *Journal of Spacecraft and Rockets,* Vol. 44, No. 6, 2007, pp. 1294.

4.McInnes, C.R., "Solar Sailing: Technology, Dynamics and Mission Applications," Springer Verlag, 1999,

5.Berg, O., and Gruen, E., "Evidence of hyperbolic cosmic dust particles(Helicentric Pioneers 8 and 9 hyperbolic cosmic dust data suggesting cosmic dust origin of previously solar effect generated noise)," *Space Research XIII,* 1973, pp. 1047-1055.

6.Burns, J., Lamy, P., and Soter, S., "Radiation forces on small particles in the solar system," *Icarus,* Vol. 40, 1979, pp. 1-48.

7.Kresak, L., "Orbital Evolution of the Dust Streams Released from Comets," *Group,* Vol. 27, No. 1, 1976, pp. 46.

8.Wie, B., "Solar Sail Attitude Control and Dynamics: Parts 1 and 2," *Journal of Guidance, Control, and Dynamics,* Vol. 27, No. 4, 2004, pp. 526-535.

9.Sohn, R., "Attitude Stabilization by Means of Solar Radiation Pressure," *ARS Journal,* Vol. 29, No. 5, 1959, pp. 371-373.

10.Acord, J., and Nicklas, J.C., "Theoretical and Practical Aspects of Solar Pressure Attitude Control for Interplanetary Spacecraft," *Progress in Astronautics and Aeronautics,* Vol. 13, 1964, pp. 73-91.

11.Cohen, D., AeroAstro, I., Gloyer, P., "Preliminary Design of a High Performance Solar Sailing Mission," *Encounter,* Vol. 200, No. 2444, 2001, pp. 260.

12.Rogan, J., Gloyer, P., Pedlikin, J., "Encounter 2001- Sailing to the stars, "*Fifteenth AIAA/USU Conference on Small Satellites, Logan, UT,* 2001.

13.Kirpichnikov, S., Kirpichnikova, E., Polyakhova, E., "Planar Heliocentric Roto-Translatory Motion of a Spacecraft with a Solar Sail of Complex Shape," *Celestial Mechanics and Dynamical Astronomy,* Vol. 63, No. 3, 1995, pp. 255-269.

14.van de Kolk, C.B., and Flandro, G.A., "Solar Sail Passive Attitude Stability and Control," *American Institute of Physics Conference Proceedings,* Vol. 552, 2001, pp. 373.

15.Falcovitz, J., "Attitude Control of a Spinning Sun-Orbiting Spacecraft by Means of a Grated Solar Sail," *Center for Space Research, MIT, CSR TR-66-17, Cambridge, MA,* 1966.

16.Lewis, D.H., Janson, S.W., Cohen, R.B., "Digital micropropulsion," *Sensors & Actuators: A.Physical,* Vol. 80, No. 2, 2000, pp. 143-154.

17.Larson, W.J., and Wertz, J.R., "Space Mission Analysis and Design," Kluwer Academic Pub, 1999,

18.Craninckx, J., and Steyaert, M., "A 1.8-GHz low-phase-noise CMOS VCO using optimized hollow spiral inductors," *Solid-State Circuits, IEEE Journal of,* Vol. 32, No. 5, 1997, pp. 736-744.